

## Research Paper

# A reservoir bathymetry retrieval study using the depth invariant index substrate cluster



Jinshan Zhu<sup>b</sup>, Bopeng Liu<sup>b</sup>, Yina Han<sup>b</sup>, Zhen Chen<sup>a</sup>, Jianzhong Chen<sup>c</sup>, Shijun Ding<sup>c</sup>, Tao Li<sup>a,\*</sup>

<sup>a</sup> Shandong Bureau of Coal Geology, Jinan, Shandong 250102, China

<sup>b</sup> College of Geodesy and Geomatics, Shandong University of Science and Technology, Qingdao, Shandong 266590, China

<sup>c</sup> Shandong Provincial Institute of Land Surveying and Mapping, Jinan, Shandong 250102, China

## ARTICLE INFO

### Keywords:

GF-2  
Sentinel-2  
Bathymetry retrieval  
DIIs  
GA

## ABSTRACT

In this paper, bathymetry retrieval is combined with the Depth Invariant Index (DII) substrate cluster to acquire more accurate water depth. DIIs are calculated through the selected samples that are in bright and dark pixels firstly. Then, substrates are clustered with DIIs by using the K-MEANS cluster algorithm. Last, in-situ data and Genetic Algorithm (GA) are applied to solve the models' parameters of the Stumpf model and the Legleiter model. The feasibility of this method is investigated in the Xia Shan Reservoir, Shandong Province, China. The experimental results show that (1) When there are various bottom types in the study area, the substrates cluster before bathymetry retrieval can significantly improve the retrieval accuracy. For example, in the without cluster case, the  $R^2$  values are both around 0.72 in the GF-2 image and the  $R^2$  values are both 0.53 in the Sentinel-2 image, and the minimum RMSE and RRMSE values are 1.09 m and 19.36 % respectively. When substrates are clustered into two clusters and three clusters,  $R^2$  values have all increased and RMSE and RRMSE values decreased. (2) Clustering substrates into more clusters may not necessarily improve retrieval accuracy. For our research area, it's better to divide the substrate into two clusters. For the two clusters case, the bathymetry result using the Legleiter model has a higher retrieval accuracy, which RMSE is 0.76 m,  $R^2$  is 0.9 and RRMSE is 11.76 %. Compared with the three clusters case, the bathymetry retrieval accuracy of the two clusters case improves more obviously.

## 1. Introduction

For thousands of years, humans have built reservoirs for a variety of purposes, including flood control, water source supply, irrigation, recreation, navigation, and hydroelectric power generation ([WCD \(World Commission on Dams\), 2000](#)). Until now, about 58,000 large reservoirs have been built globally. There is no doubt that reservoirs play a vital role in sustainable human development. On the one hand, large reservoirs are estimated to contribute to 12 %-16 % directly of global food production. Recent predictions show that 70 % more food will be needed by 2050 to accommodate a 40 % increase in the world's population and to adapt to expected changes in global dietary patterns. A part of this additional food will be produced on irrigated land, requiring an 11 % increase in the amount of needed water, much of which is likely to come from reservoirs ([WCD \(World Commission on Dams\), 2000](#)). On the other hand, reservoirs can reduce the enormous losses incurred by industrial development, such as changes in water and food security, and an

increase in the incidence of infectious diseases.

From the above, the role of reservoirs cannot be separated from the provision of water resources. Although most of the Earth is covered by water, less than 1 % of the planet's total freshwater resources are directly accessible to humans. Developing and least-developed countries are likely to fail to access water universally owing to increased surface water shortfall ([Bo et al., 2021](#)). In addition, global population growth, increased land utilization rate, achievement of per capita consumption levels, and climate changes are imposing enormous pressures on the availability of freshwater resources ([Guo et al., 2021](#)). Therefore, the monitoring of reservoir ecosystems is becoming increasingly important.

In China, the government is also increasingly focusing on monitoring the ecology of reservoirs. In recent years, as the largest reservoir in Shandong Province, the Xia Shan reservoir has many threats due to upstream industries, domestic sewage, garbage pollution, and agricultural pollution. These factors alter the bathymetry in Xia Shan Reservoir and the water environment. At present, the water ecological

\* Corresponding author.

E-mail address: [sdzmchy\\_litao@163.com](mailto:sdzmchy_litao@163.com) (T. Li).

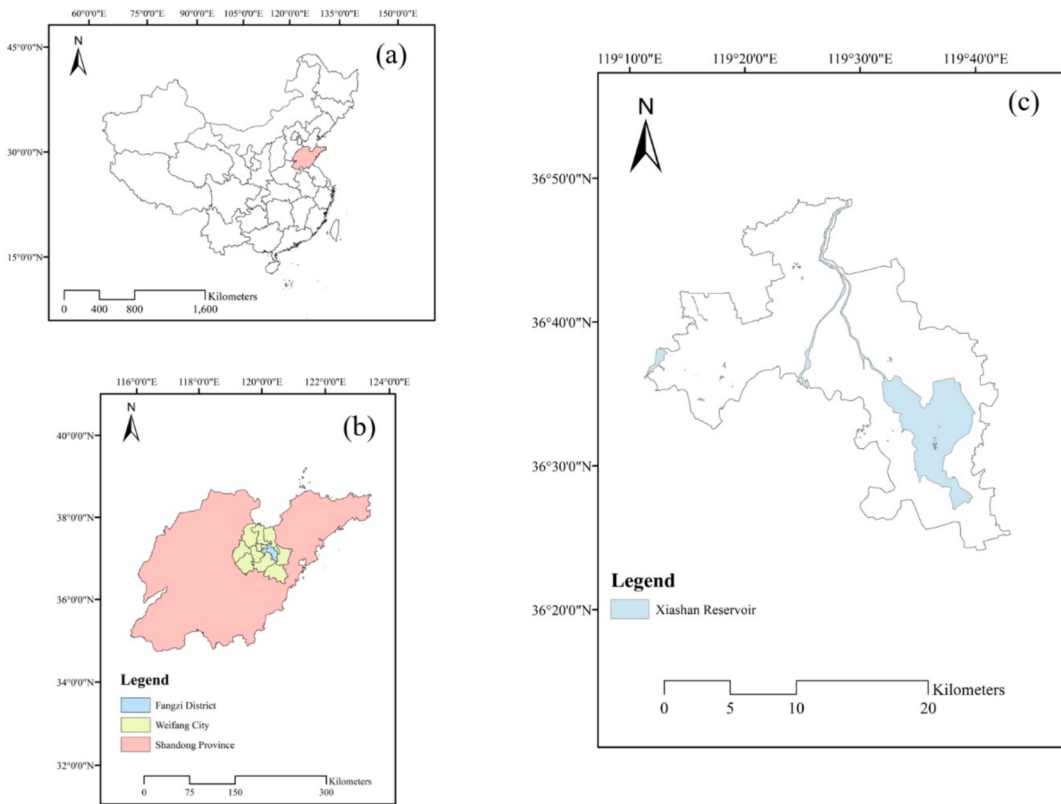


**Fig. 1.** Location of the study area.

environment monitoring and remediation of Xia Shan Reservoir have become a key research target in Shandong Province, China.

Bathymetry is one of the important parameters in hydrologic studies and aquatic environmental changes and is commonly measured using sonar (Chen et al., 2019). Traditional bathymetry measurements are highly precise but costly and time-consuming. With the development of remote sensing technology, many researchers have used remote sensing images to replace traditional bathymetric measurements.

As a result, many bathymetric models have been rapidly developed (Ma et al., 2018). Currently, the retrieval methods are classified as empirical, semi-empirical, analytical, and semi-analytical based on statistical, bio-optical, and physics-optical properties. Semi-empirical methods based on the radiative transfer equation (RT) for light require in-situ data statistical correction (Ashphaq et al., 2021). Among semi-empirical methods, Stumpf's log-linear models are more widely used (Di et al., 1999; Polcyn and Sattinger, 1969; Polcyn and Lyzenga, 2013). Although, according to Stumpf's research, the effect of different substrates can be eliminated by using a ratio to some extent, accurate water bathymetry is usually hard to obtain without distinguishing the substrate types when different substrate types with obvious different spectrums exist. Substrate cluster is a difficult problem to deal with. So far, there are several ways to identify types of substrates. The most common method is acoustic detection by shipboard equipment (Reshitnyk et al., 2014), but substrate identification is difficult in areas that are difficult for ships to reach. In 1981, Lyzenga (Lyzenga, 1978) proposed that the Depth Invariant Index (DII) could be used to classify substrates. The method can categorize substrates without considering the water environment. Many studies are confirming the effectiveness of this method to categorize substrates. For example, Manessa et al (Manessa et al., 2016) used this method to map the substrate near Indonesia successfully. Poursanidis et al (Dimitris et al., 2019) and Suo et al (Suo et al., 2019) also applied DII for water column correction and the results are very excellent. Consequently, many researchers have combined this method of substrate cluster with bathymetric retrieval to improve the

accuracy of bathymetric retrieval. Zhu et al (Zhu and Yin, 2022) successfully improved the bathymetric retrieval accuracy of Ganquan Island in Xisha Islands, China, by adding DIIs and Location features to the Back Propagation (BP) neural network and Random Forest (RF) neural network. Similarly, Cheng et al (Cheng et al., 2021) combined the empirical model with the DIIs to obtain satisfactory results in the Xisha Islands.

In this paper, there are two main objectives: Most of the previous research works have explored the validity of applying the DII index for substrate cluster and have also investigated that the DII index can improve the accuracy of bathymetry retrieval in Case I waters, however none of these researches have investigated the effect in the Inland waters. Therefore, the first objective is assessing the potentiality of using DII for substrate cluster and bathymetry retrieval in the Inland waters. The second objective of this research is to derive a suitable bathymetry retrieval model for the Xia Shan Reservoir by comparing the linear Stumpf model with the nonlinear Legleiter inversion model based on the first objective.

To achieve these two objectives, the study area substrates are divided into two and three clusters by DIIs and the K-MEANS cluster algorithm first. Secondly, the GA algorithm is applied to optimize the model parameters to obtain the predicted bathymetry. Finally, to better assess the performance of our method that using DIIs for bathymetry retrieval, the accuracy of bathymetry retrieval results obtained by the two models in the study area with and without substrate clusters are compared, respectively.

## 2. Research area and data

### 2.1. Study area

The study area used for this experiment is the Xia Shan Reservoir (Fig. 1). The construction of Xia Shan Reservoir started in November 1958 and was completed in 1960. The reservoir is located in Shandong

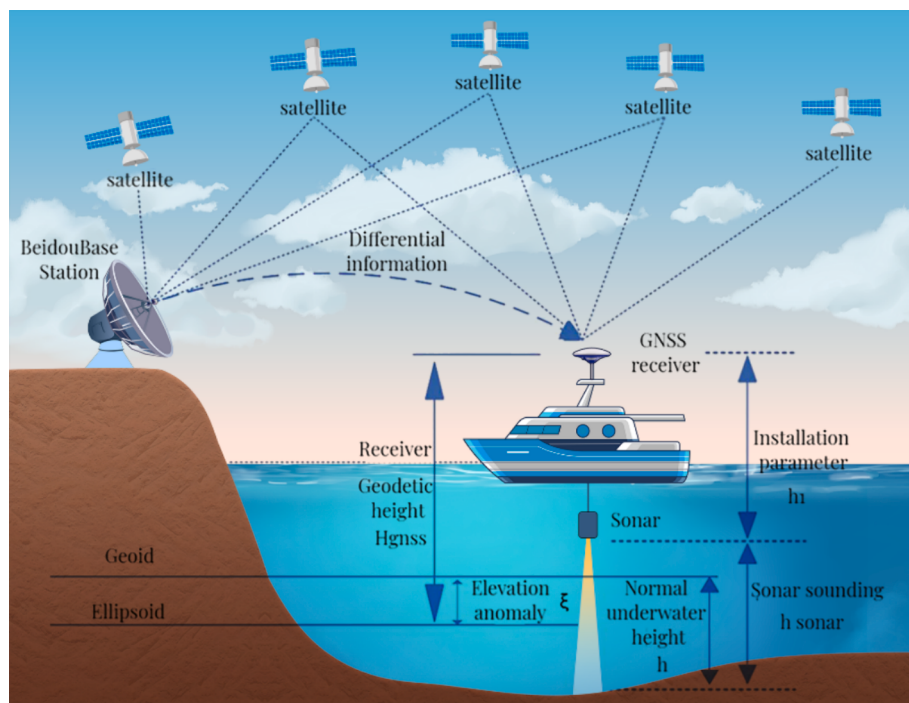


**Fig. 2.** Schematic diagram for obtaining measured data.

Province, China, 50 km southeast of Weifang city. It covers an area of 144 square km and it has a water depth of 0 m to 11 m, with an average depth of about 5 m and relatively good water quality. With a watershed area of 4210 square km and a total capacity of 1,405 million cubic meters, the reservoir is the largest in Shandong Province.

## 2.2. Data

This experiment combines remote sensing images with in-situ data to verify that substrate clusters can improve the accuracy of bathymetric inversion in the Xia Shan Reservoir. The in-situ data was provided by Shandong Provincial Institute of Land Surveying and Mapping. Remote sensing images are employed with GF-2 and Sentinel-2 satellite images. Details are as follows.

### 2.2.1. Field data

The in-situ water depth data without tidal correction is offered by Shandong Continuously Operating Reference Stations (SDCORS). As shown in Fig. 2, a single-beam echo sounder firstly is used to obtain  $h_{sonar}$ . During  $h_{sonar}$  collection, the direction of the survey line is perpendicular to the direction of the same Isobaths line, and the direction of the check line is perpendicular to the survey line. Then, the same accuracy test is carried out using check line data. The result shows that the accuracy of the  $h_{sonar}$  data was  $\pm 0.11$  m. Then  $H_{gnss}$  is obtained by using GNSS receivers. The installation parameters  $h_1$  is obtained by the hardware setup, and the elevation error,  $\epsilon$ , is offered by the Shandong Province vertical reference. At last, the water depth,  $h$ , can be derived according to Eq.1.

$$h = H_{gnss} - h_1 - h_{sonar} - \epsilon \quad (1)$$

### 2.2.2. Remote sensing images

The optical Sentinel-2 image, acquired on July 20, 2020, encompassed 13 spectral bands spanning the visible/near-infrared and short-wave infrared spectral ranges. The spatial resolution of the image is 10 m in the visible and near-infrared spectral ranges, providing valuable information for bathymetry retrieval. In addition, a GF-2 image was used to validate the method in the paper. To retrieve the water depth

accurately, the remote sensing image with the least cloud is selected and the data acquisition time is as close as possible to the in-situ water depth. Therefore, an image acquired on June 7, 2019, with a cloud of 0 % is adopted for bathymetry retrieval.

## 3. Methodology

In the Xia Shan Reservoir area, the bathymetry retrieval experiment combined with the DII substrate cluster comprises three main steps, as shown in Fig. 3. The first step involves preprocessing the GF-2 and Sentinel-2 images. In the next step, the DII models are constructed by selecting pixel samples in GF-2 and Sentinel-2 images, respectively. Then, DIIs and K-Means cluster algorithm are applied to the substrates cluster. In the third step, applying the GA optimization algorithm is to solve the parameters of the Stumpf and the Legeleiter models for establishing bathymetry retrieval models. Then, compare the accuracy of bathymetry retrieval between with and without clustering substrates by plotting scatter plots.

### 3.1. Satellite image preprocessing

The first step includes preprocessing the GF-2 and Sentinel-2 images. Since the digital values (DN) in the raw GF-2 remote sensing images are dimensionless and physically meaningless, radiometric calibration is necessary to convert the DN values into radiance. In this paper, absolute radiometric is adopted according to gain and bias values offered by the official website of GF-2. In addition, atmospheric correction is also a critical step for quantitative remote sensing. In this research, the Second Simulation of the Satellite Signal in the Solar Spectrum (6S) radiative transfer model is used to accomplish this task. The Py6s python package, which is a Python interface to the 6S Radiative Transfer Model is offered by Robin Wilson (<http://www.py6s.rtwilson.com>). The Py6s python package has already included several typical atmospheric models, aerosol type models, and spectral response functions of commonly used sensors, spectral response of the GF-2 sensor is also included in this package (Shang et al., 2021). So, it can be used for GF-2 atmospheric correction directly. Many parameters such as the sensor zenith and azimuth angles, solar zenith and azimuth angles, date, central latitude and

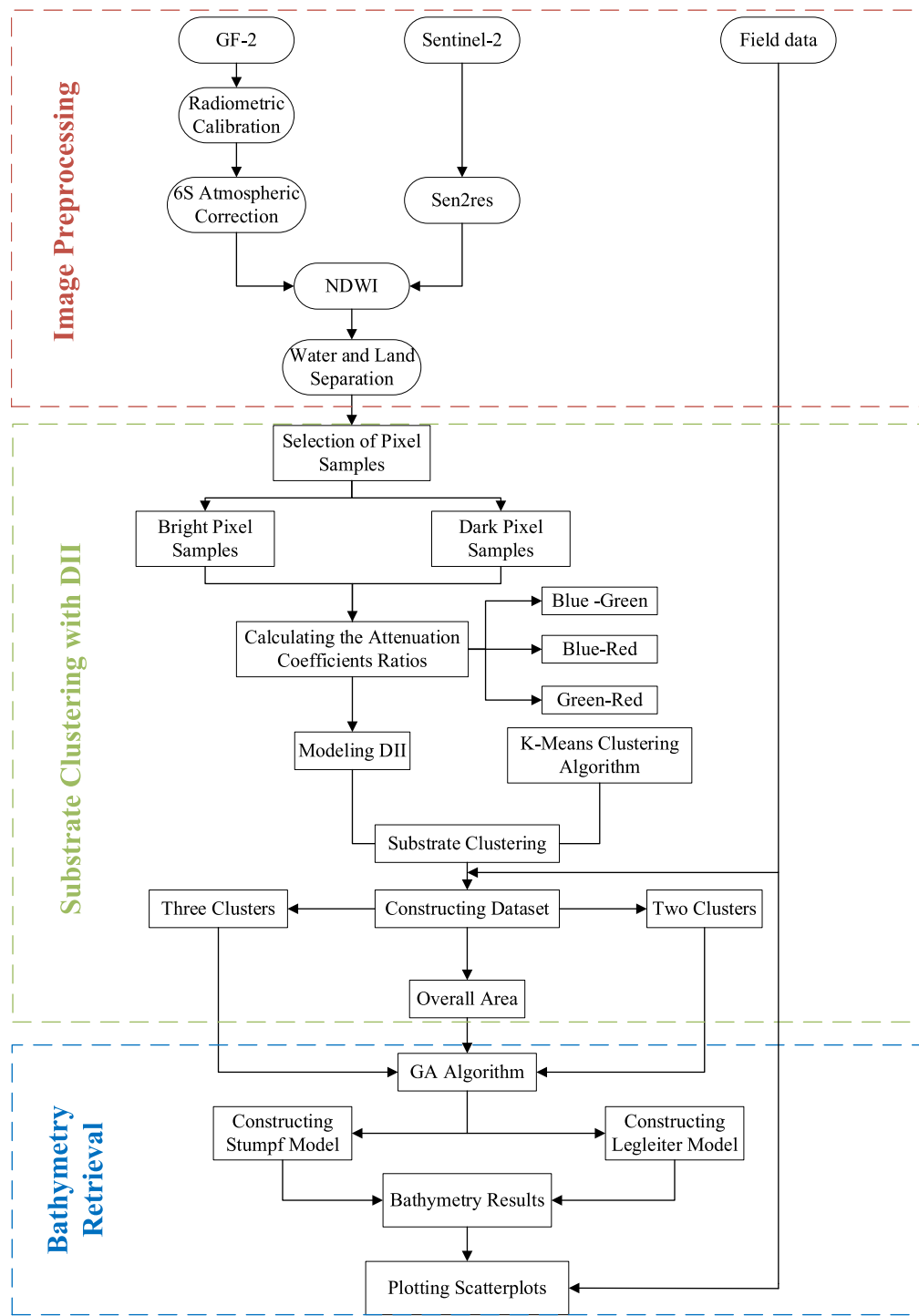


Fig. 3. Flowchart of bathymetry retrieval with DII substrate cluster.

longitude, mid-latitude summer atmospheric mode type, urban aerosol type, aerosol optical thickness aot550, altitude of the study area and satellite sensor orbit altitude, etc. are necessary to run the python package. Correction factors, which are listed in, can be obtained after running Py6s. Then the water surface reflectance, R, can be calculated according to Eq.2 (Zhao et al., 2021). This reflectance is used further for water depth modeling.

$$R = \frac{(X_a * L - X_b)}{1 + X_c * (X_a * L - X_b)} \quad (2)$$

where R is the corrected water surface reflectance,  $x_a, x_b, x_c$  is the

correction factor, and L is the radiance obtained from radiometric correction.

The Sentinel-2 image used in this experiment is a Level 2A product so atmospheric correction is not required. Then, the Level 2A product, which includes surface reflectance values, is resampled to a 10 m spatial resolution by the Sen2Res tool.

To conduct the experiments more accurately, NDWI (Normalized Difference Water Index) was calculated on the preprocessed images for extracting the Xia Shan Reservoir area.

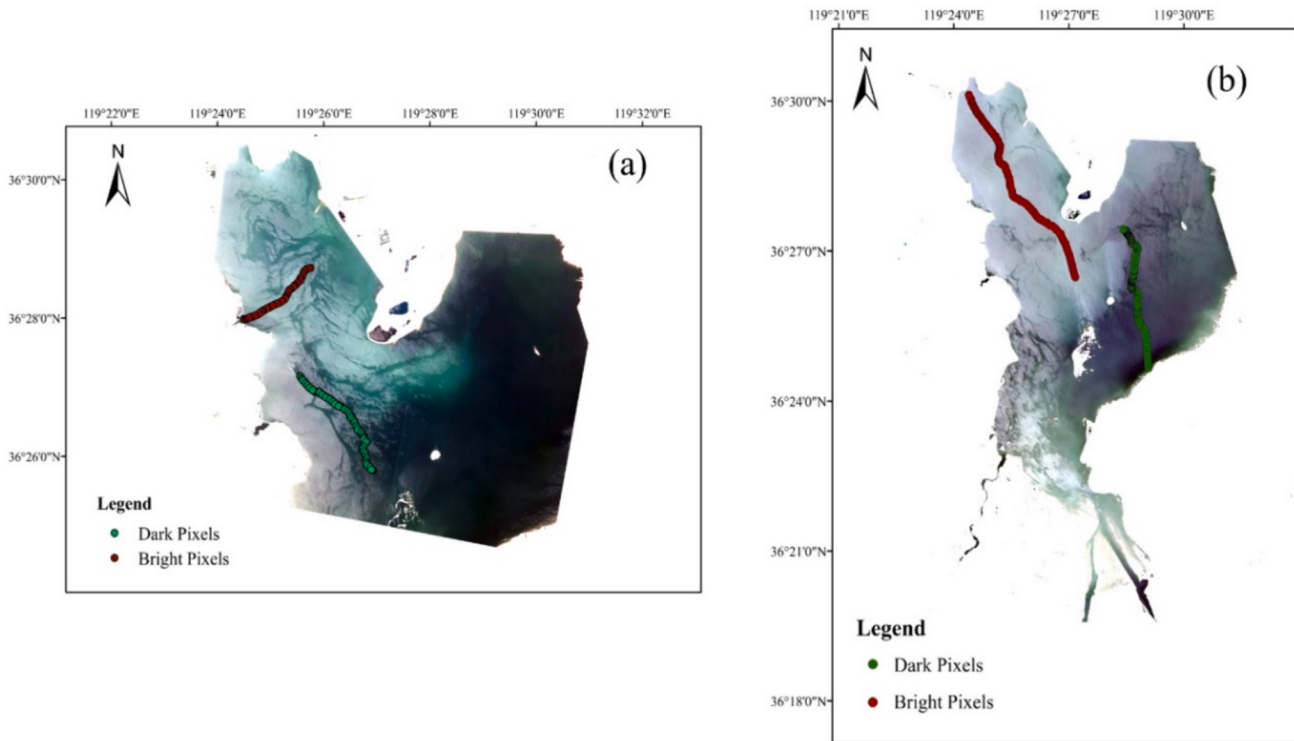


**Fig. 4.** Sample point distribution of bright and dark pixels: (a) GF-2, and(b) Sentinel-2.

$$NDWI = \frac{(R_{B2} - R_{B4})}{(R_{B2} + R_{B4})} \quad (3)$$

where  $R_{B2}$  is the reflectance of the green band,  $R_{B4}$  is the reflectance of the red band.

### 3.2. Modeling DII

After extracting the study area from GF-2 and Sentinel-2 images, it is necessary to select the bright and dark pixel samples to establish the DII models. The samples are shown in Fig. 4.

Fig. 4 shows true color images in Xia Shan Reservoir of GF-2 and Sentinel-2 satellites. According to these two images, it is obvious that there are bright and dark two kinds of different substrates. So, a substrate cluster is necessary before bathymetry retrieval. In this research, two groups of samples, bright and dark, are selected by visual interpretation. Then, two datasets for further substrate clusters are obtained. In this dataset, there are 58 samples for bright pixels and 252 samples for dark pixels in the GF-2 image, and there are 77 samples for bright and 113 samples for dark pixels in the Sentinel-2 image.

The DII used in this experiment was proposed by Lyzenga (Lyzenga, 1978) in 1978. Equation 4 (Manuputty, 2017) shows that DII is related to the ratio of the attenuation coefficient and the reflectance of the two bands. When the inherent optical properties (IOPs) of the water column are homogeneous,  $k_i/k_j$  is a constant, DII is only dependent on reflectivity. So, substrates with different reflectance correspond to different DII.

$$DII = \ln(R_i) - (k_i/k_j) \cdot \ln(R_j) \quad (4)$$

where  $R_i$  and  $R_j$  are the corrected remote sensing reflectance of the two bands,  $k_i/k_j$  is the ratio of attenuation coefficients.

According to the National Monthly Report on Surface Water Quality in June 2023 offered by the Ministry of Ecology and Environment of the People's Republic of China, the water of the Xia Shan Reservoir is clear. The study area can cluster substrates by DII.

To calculate the DII,  $k_i/k_j$  should be determined firstly, as shown in Eq.5 and Eq.6 (Manuputty, 2017).

$$k_i/k_j = a + \sqrt{(a^2 + 1)} \quad (5)$$

$$a = (\sigma_{ii} - \sigma_{jj}) / 2\sigma_{ij} \quad (6)$$

where  $\sigma_{ii}$  and  $\sigma_{jj}$  are the variances of bands  $i$  and  $j$ ,  $\sigma_{ij}$  is the covariance.

### 3.3. Bathymetry retrieval models

In this research, two empirical models, the Stumpf logarithmic ratio model, and the Legleiter nonlinear model are employed for water depth retrieval. The Stumpf model is one of the widely bathymetric retrieval models, which requires only three model parameters. As shown in Eq.7, Stumpf (Stumpf et al., 2003) found a linear relationship between water depth between water and blue and green band reflectance. However, this relationship is only obvious in specific areas of shallow water. As depth increases, the nonlinear relationship presents more between depth and reflectivity (Cahalane et al., 2019). Thus, Legleiter (Legleiter, 2021) proposed a nonlinear model by modifying the Stumpf model, as shown in Eq.8.

$$Z = m_1 \frac{\ln(n \bullet R_w(\lambda_i))}{\ln(n \bullet R_w(\lambda_j))} - m_0 \quad (7)$$

$$Z = m_2 \left( \frac{\ln(n \bullet R_w(\lambda_i))}{\ln(n \bullet R_w(\lambda_j))} \right)^2 + m_1 \left( \frac{\ln(n \bullet R_w(\lambda_i))}{\ln(n \bullet R_w(\lambda_j))} \right) + m_0 \quad (8)$$

In Eq.7, and Eq.8,  $Z$  is the retrieval water depth,  $m_0$ ,  $m_1$ ,  $m_2$  are empirical parameters,  $n$  is a constant which is generally set to 1000,  $R_w(\lambda_i)$  and  $R_w(\lambda_j)$  are the water surface reflectance of blue and green bands, respectively.

**Table 1**  
Ratio of attenuation coefficients for each band pair.

RS image	Band	Pixel	$k_i/k_j$	Average
GF-2	Blue-Green	Bright	0.99697	0.99778
		Dark	0.99858	
	Blue-Red	Bright	0.99345	0.99595
		Dark	0.99846	
	Green-Red	Bright	0.99522	0.99743
		Dark	0.99965	
Sentinel-2	Blue-Green	Bright	1.13560	0.94821
		Dark	0.76083	
	Blue-Red	Bright	1.02518	0.96247
		Dark	0.89975	
	Green-Red	Bright	0.82069	0.94060
		Dark	1.06051	

**Table 2**  
DII models for the Xia Shan reservoir.

RS image	Pairs of bands	DII
GF-2	Blue-Green	$DII_{BG} = \ln(b1) - 0.99778\ln(b2)$
	Blue-Red	$DII_{BR} = \ln(b2) - 0.99595\ln(b3)$
	Green-Red	$DII_{GR} = \ln(b1) - 0.99743\ln(b3)$
Sentinel-2	Blue-Green	$DII_{BG} = \ln(b1) - 0.94821\ln(b2)$
	Blue-Red	$DII_{BR} = \ln(b2) - 0.96247\ln(b3)$
	Green-Red	$DII_{GR} = \ln(b1) - 0.94060\ln(b3)$

### 3.4. Optimization algorithms

In bathymetry retrieval, the model parameters determine the accuracy of retrieval, which is solved using the GA. The GA algorithm efficiently navigates wide search spaces to discover optimal solutions by employing genetic techniques- selection, crossover, and mutation of a group of potential solutions (referred to as chromosomes or individuals) for a given problem (Goldberg and Holland, 1988). Based on a specific fitness function criterion, the algorithm selects the most suitable parameters in the population, composes them, and changes them to produce a new generation of candidate parameters. At last, the algorithm selects the most suitable parameters for bathymetry prediction and improves the inversion accuracy.

In this study, the GA optimization algorithm is executed by applying training samples, which are randomly selected from field data. The training sample points are used to optimize the fitness function, which reaches a minimum value to obtain the most optimum parameters for bathymetry retrieval models. The fitness function is defined as Root Means Square Error (RMSE), as shown in Eq.9.

### 3.5. Accuracy assessment

In this paper, three metrics, as shown in Eq. 9–11 were used. Among them, since the values of water depths are negative, the absolute value is taken for the RRMSE.

Root Means Square Error (RMSE):

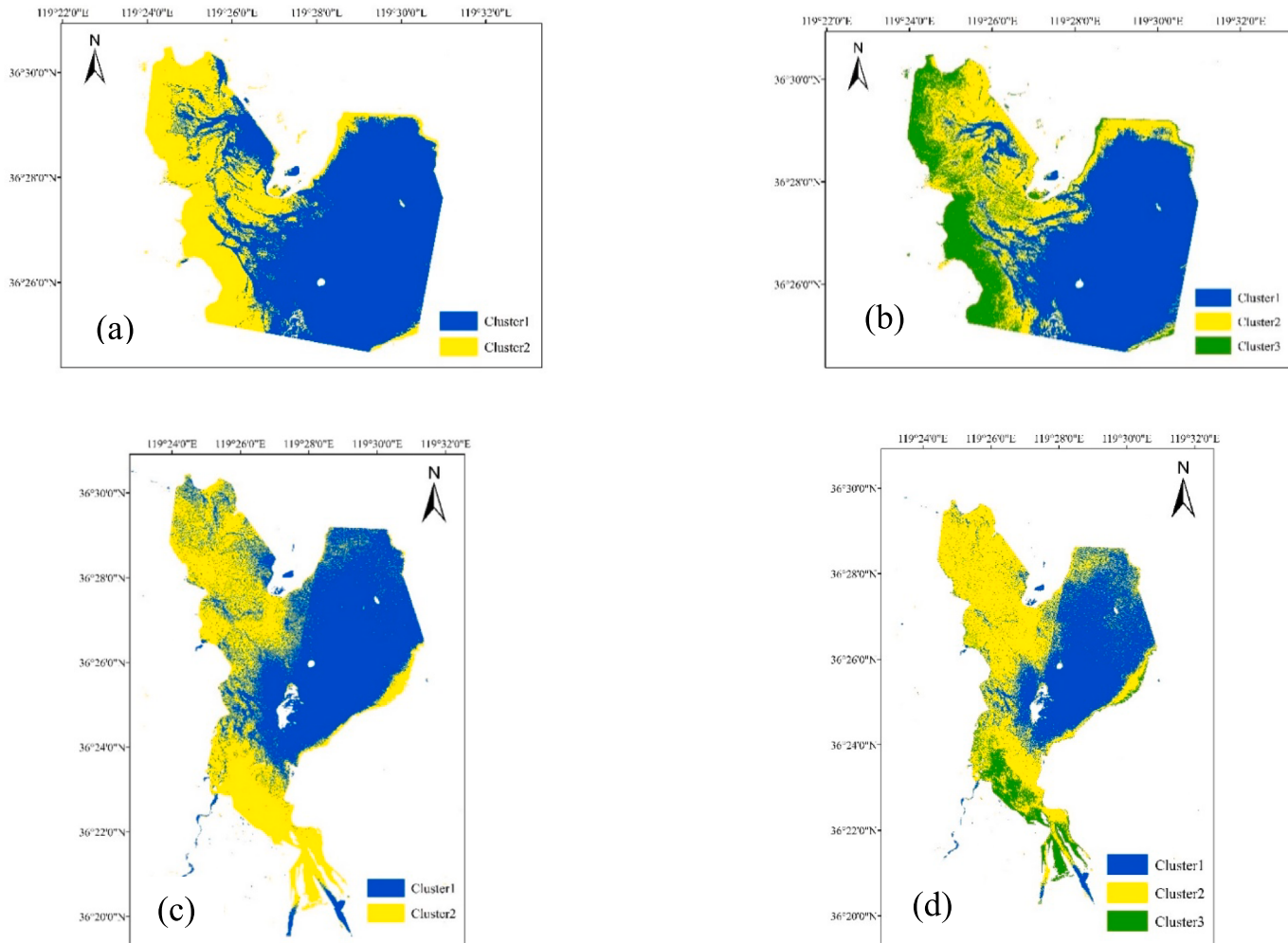


**Fig. 5.** Substrate cluster map: (a), (b) GF-2 two clusters and three clusters, and (c), (d) Sentinel-2 two clusters and three clusters.

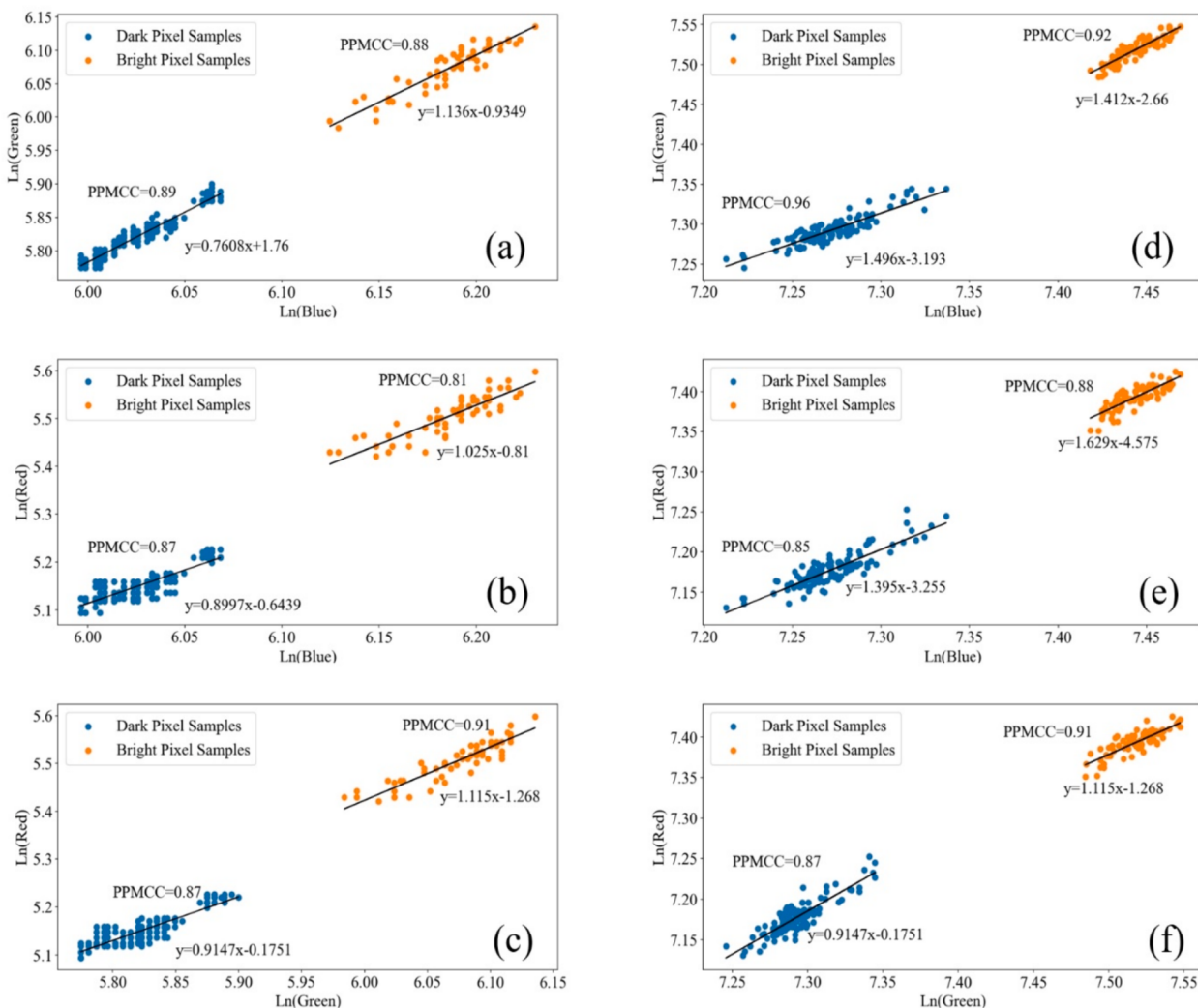


**Fig. 6.** Natural logarithmic scatterplot of bright and dark image element sample points on each band pair: (a)-(c) GF-2 samples, (d)-(f) Sentinel-2 samples.

**Table 3**  
Accuracy of substrate cluster.

RS image	Cluster	Kappa coefficient	Overall accuracy
GF-2	Two	0.994	99.78 %
	Three	0.683	81.48 %
Sentinel-2	Two	0.885	94.30 %
	Three	0.929	95.74 %

**Table 5**  
Bathymetry retrieval samples in Sentinel-2.

	Total	Two clusters		Three clusters		
		Cluster1	Cluster2	Cluster1	Cluster2	Cluster3
Control points	304	120	200	70	154	80
Checkpoints	188	54	118	40	100	48
Overall	492	174	318	110	254	128

**Table 4**  
Bathymetry retrieval samples in GF-2.

	Total	Two clusters		Three clusters		
		Cluster1	Cluster2	Cluster1	Cluster2	Cluster3
Control points	220	120	100	100	70	32
Checkpoints	134	64	70	72	48	32
Overall	354	184	170	172	118	64

$$RMSE = \sqrt{\frac{\sum_{i=1}^n (z_i - \hat{z}_i)^2}{n}} \quad (9)$$

Relative Root Mean Square Error (RRMSE):

$$RRMSE = \left| \frac{RMSE}{\sqrt{\frac{\sum_{i=1}^n z_i}{n}}} \right| \quad (10)$$

Coefficient of Determination ( $R^2$ ):

$$R^2 = \frac{\sum_{i=1}^n (z_i - \bar{z})^2 - \sum_{i=1}^n (z_i - \hat{z}_i)^2}{\sum_{i=1}^n (z_i - \bar{z})^2} \quad (11)$$

where  $z_i$  is the in-situ bathymetric value of the sample point,  $\hat{z}_i$  is the

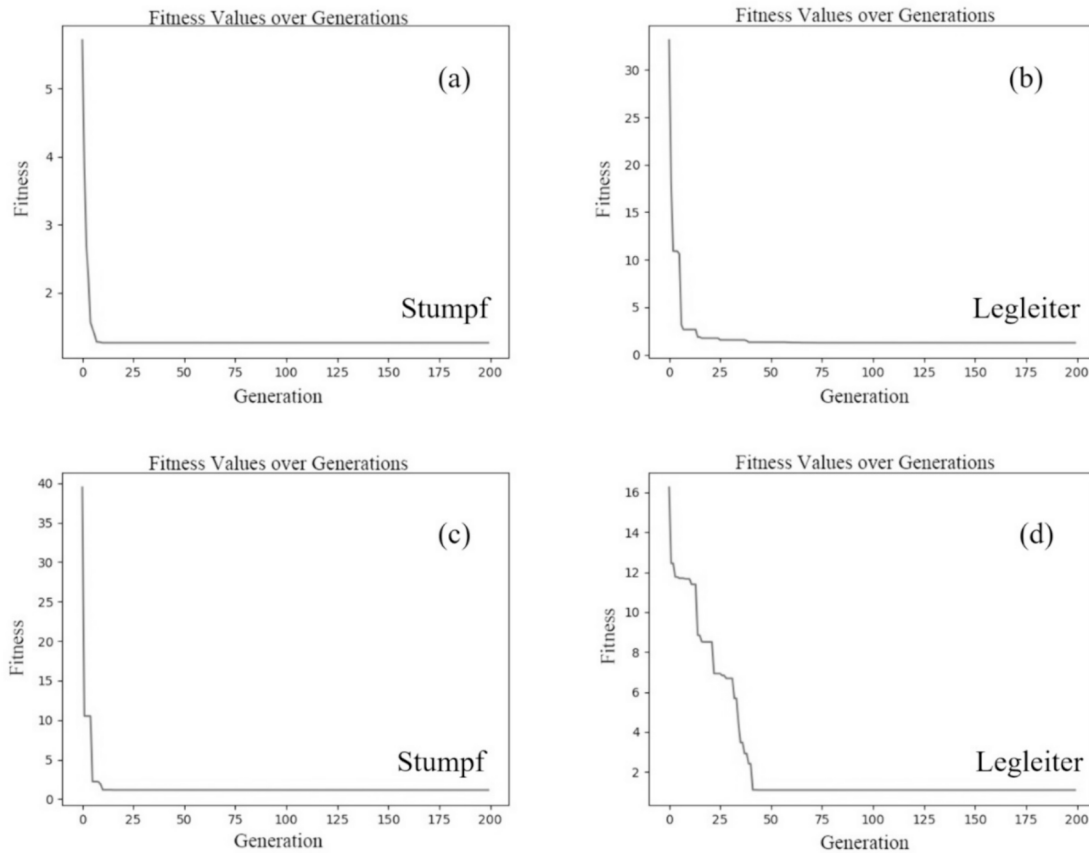


**Fig. 7.** Fitness values versus generation in parameter solution without clustering: (a), (b): GF-2, and (c), (d): Sentinel-2.

retrieved bathymetric value of the sample point,  $\bar{z}$  is the average bathymetric value of the sample point,  $n$  is the number of sample points.

#### 4. Result

In this section, cluster results are shown and accuracy is evaluated first. Then, retrieval results with and without clusters are evaluated, which proves the effectiveness of substrate clusters for improving retrieval accuracy.

##### 4.1. Substrate cluster

Before clustering, bands of the selected dataset are composed into blue-green, blue-red, and green-red band pairs for calculating  $k_i/k_j$ , as shown in Table 1. The average is used to calculate DIIs, as shown in Table 2. DIIs are used to further divide the study area into two clusters and three clusters by the K-MEANS cluster algorithm, as shown in Fig. 5.

For evaluating cluster accuracy, the correlation of the bright and dark pixel samples is assessed by using Pearson Product Moment Correlation Coefficient (PPMCC), as shown in Eq. 12. Fig. 6 plots the scatter distribution of reflectance of each band pair. It can be seen that the PPMCC values of the three band pairs (blue-green, blue-red, and green-red) are all over 0.8 in the GF-2 image and the PPMCC values of the three band pairs are all close to 0.9 in the Sentinel-2 image, which indicates that the selected pixel samples of this experiment have strong correlations. Then, the accuracy and kappa coefficients are displayed in Table 3.

$$\text{PPMCC} = \frac{\text{cov}(B_i, B_j)}{\sigma_{B_i} \sigma_{B_j}} \quad (12)$$

where  $\text{cov}(B_i, B_j)$  is the covariance of bands  $i$  and  $j$ ,  $\sigma_i$  and  $\sigma_j$  are the

variances of bands  $i$  and  $j$ .

##### 4.2. Bathymetry retrieval result

In this study, the parameter solution is performed through the GA function from the scikit-opt library. The GA function is configured for 200 generations with a population size of 50, a crossover probability of 0.5, and a mutation probability of 0.01. Parameter solution is conducted on selected filed bathymetry data which is shown in Table 4 and Table 5 in the GF-2 image and Sentinel-2 image. Fig. 7 illustrates the fitness function plot for 200 generations of parameter solutions for all regions and the diagrams of the fitness function after the cluster are presented in Fig. 8. Based on Fig. 7 and Fig. 8, it is clear that the GA algorithm achieves the minimum fitness values in all cases after 200 generations. They also show that both bathymetric inversion models get the best parameters in each category after 200 generations.

##### 4.2.1. Bathymetry accuracy without cluster

To demonstrate retrieval effectiveness with cluster, the accuracy of bathymetry retrieval without cluster is evaluated first. From Fig. 9, it can be seen that retrieval results without cluster are unsatisfactory,  $R^2$  is 0.53 in Sentienl-2 with Stumpf model, the minimum of RMSE is 1.09 m. The RRMSE values are both close to 20 % in the GF-2 image and the RRMSE values are close to 25 % in the Sentinel-2 image. The retrieval results are all underestimated from -8m to -10 m, and they are concentrated in the same depth range.

##### 4.2.2. Bathymetry accuracy with cluster

In this section, retrieved bathymetry results with two and three substrate clusters are first evaluated, respectively. Then, retrieval results without clusters and with two clusters are compared. At last, retrieval results with two and three clusters were redisussed.

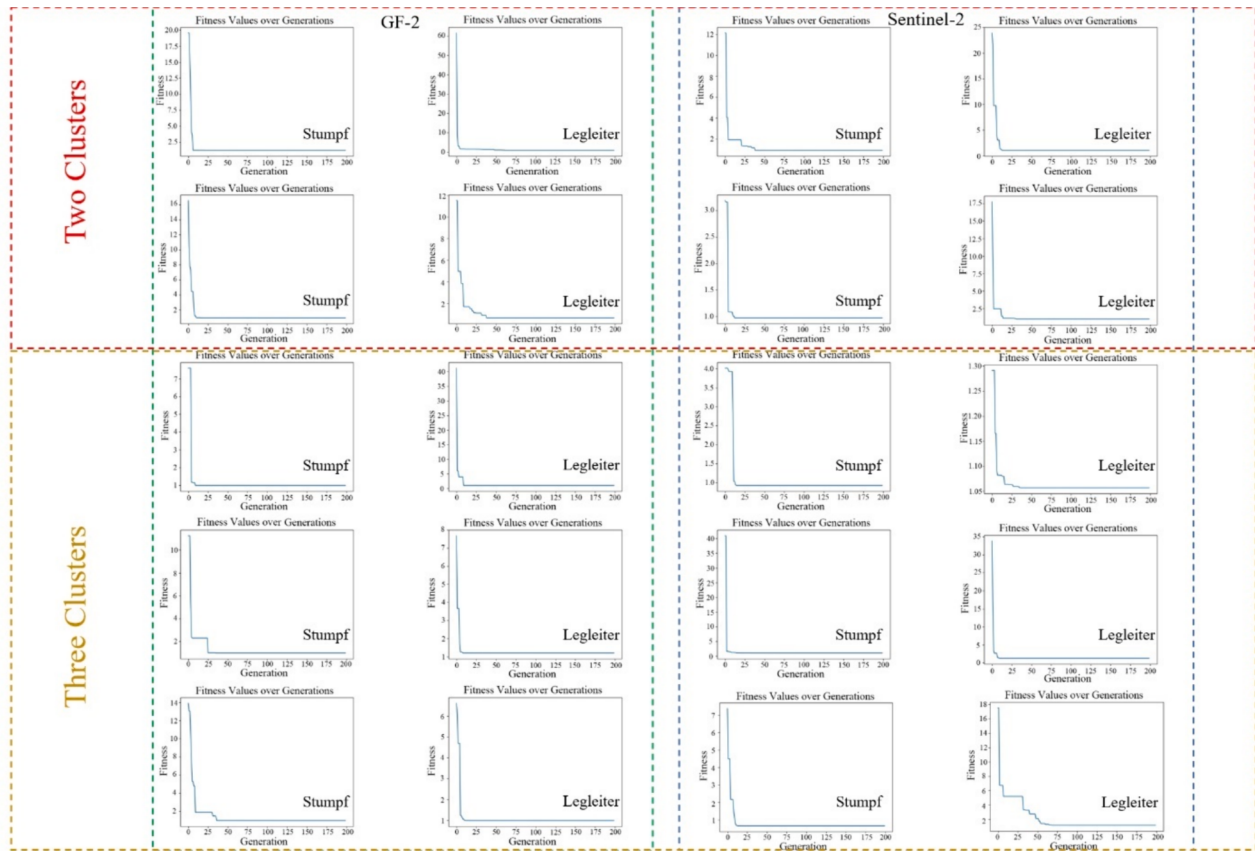


**Fig. 8.** Fitness values versus generation in parameter solution with clustering.

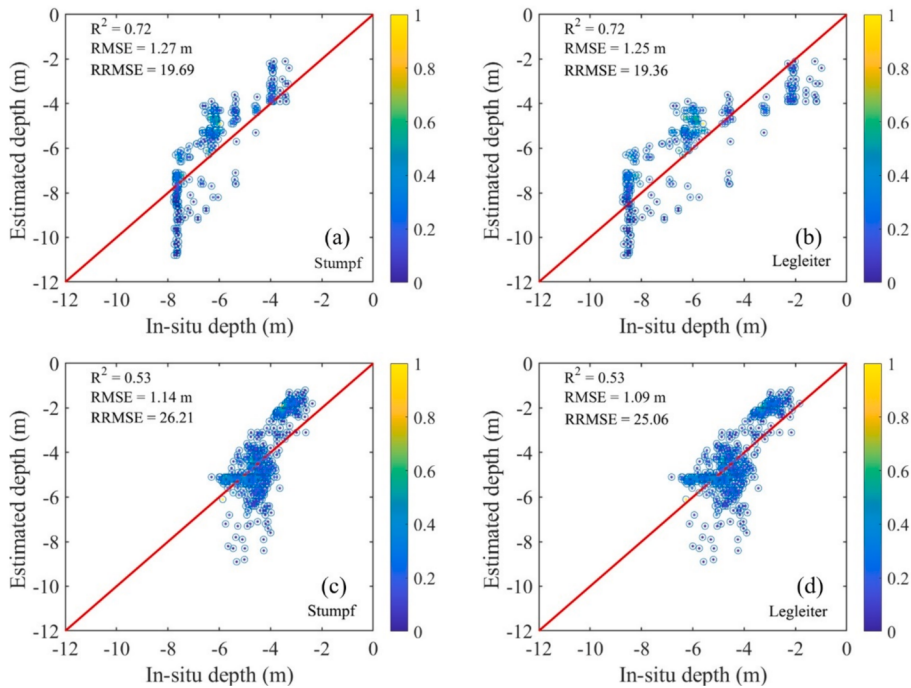


**Fig. 9.** Scatterplot of the overall bathymetric retrieval without cluster: (a), (b) Inversion of bathymetry with Stumpf model and Legleiter model separately in GF-2 and (c), (d) Inversion of bathymetry with Stumpf model and Legleiter model separately in Sentinel-2.

For two substrate cluster cases, as shown in Fig. 10, the results using the Legleiter model (Fig. 10(b) and (d)) are better than those using the Stumpf model (Fig. 10(a) and (c)). For example, the  $R^2$  with the Legleiter

model using the GF-2 image (Fig. 10(b)) is 0.9 and that of the Stumpf model using the GF-2 image (Fig. 10(a)) is 0.78 and the RRMSE with the nonlinear model using the GF-2 image decreases from 19.36 % to 11.76

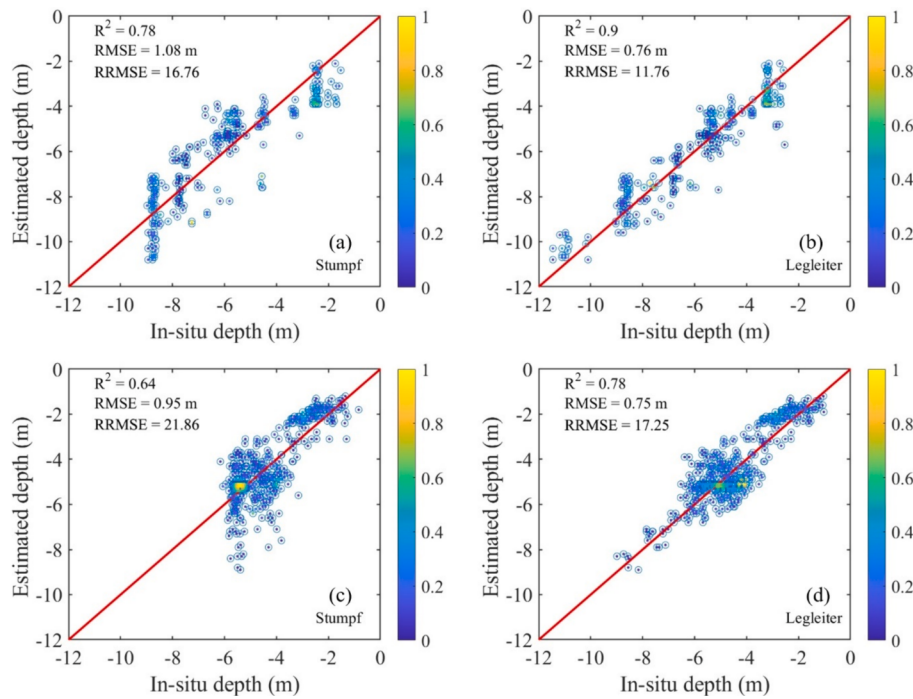


**Fig. 10.** Scatterplot of the overall bathymetric retrieval with two clusters: (a), (b) Inversion of bathymetry with Stumpf model and Legleiter model separately in the GF-2, and (c), (d) Inversion of bathymetry with Stumpf model and Legleiter model separately in the Sentinel-2.

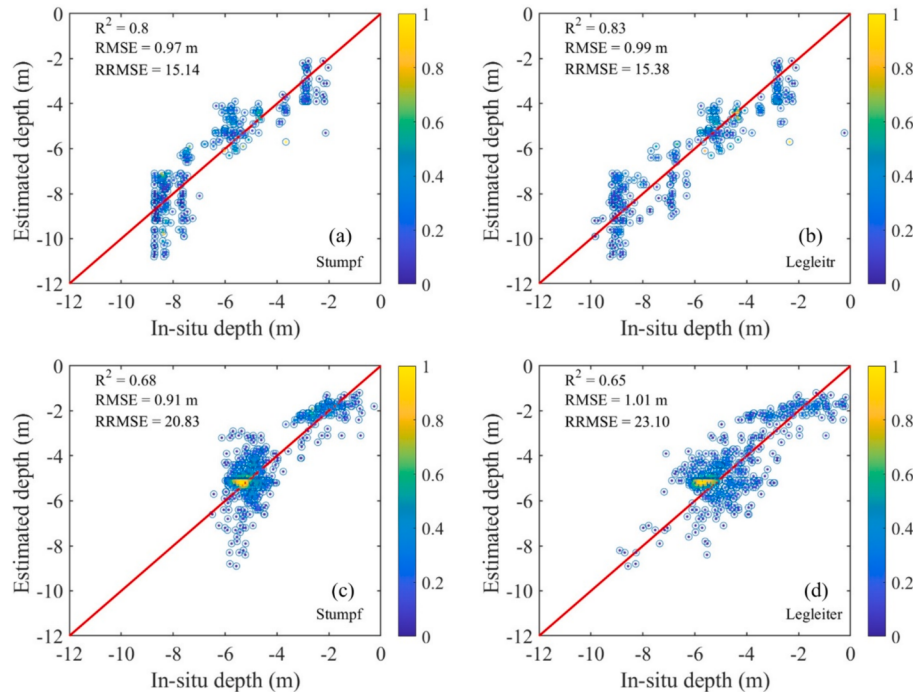


**Fig. 11.** Scatterplot of the retrieval of the overall bathymetric with three clusters: (a), (b) Inversion of bathymetry with Stumpf model and Legleiter model separately in GF-2 and (c), (d) Inversion of bathymetry with Stumpf model and Legleiter model separately in Sentinel-2.

%, the improvement is very obvious. According to the RMSE, the improvement is also obvious, RMSE in Fig. 10(b) is reduced by 29.6 % compared to that of Fig. 10(a). Fig. 10(c) and Fig. 10(d) also have the similar improvement. It is worth noting that in the depth range of -8m to -10 m in Fig. 10(a) and Fig. 10(c), the predicted depths are all clustered in the same range, which is also consistent with the Stumpf model's prediction of deep regions. Subsequently, as shown in Fig. 10(c) and Fig. 10(d), it is clear that the problem of inverting Stumpf's linear

model is solved when applying a nonlinear model to invert the bathymetry in deep water.

For three bottom clusters, as shown in Fig. 11(a) and Fig. 11(b), the nonlinear model predicts water depths that are not significantly improved compared to the linear model in deep water. To compare Fig. 11(a) with Fig. 11(b), the RMSE and the RRMSE of the Legleiter model are higher than those of the linear model. To compare Fig. 11(c) with Fig. 11(d), the RMSE and the RRMSE of the Stumpf model are also

higher than those of the linear model.

The comparisons between Fig. 9, Fig. 10, and Fig. 11 show that retrieval results all have a substantial improvement after the cluster. Among them, the retrieval results with two clusters are elevated the greatest. To compare Fig. 10(b) with Fig. 9(b), the  $R^2$  of the Legleiter model using GF-2 is 0.9 and the RMSE is 0.76 m. The  $R^2$  has an improvement of 25 % and the RMSE has a reduction of 39.2 %. The RRMSE decreased from 19.36 % to 11.76 %. The improvement is very significant from these evaluations. However, for three clusters, the elevation effect is not as noticeable as the two clusters. To compare Fig. 11(b) with Fig. 10(b) and Fig. 9(b), the  $R^2$  of the Stumpf model using GF-2 is 0.83, the RMSE is 0.99 m and the RRMSE is 15.38 %. From these evaluation metrics, it can be seen that although the inversion accuracy with three clusters is improved compared to the inversion accuracy without clustering, the inversion accuracy is decreased compared to the inversion accuracy with two clusters. This also indicates that the substrate is divided into more clusters does not improve the retrieval accuracy.

## 5. Discussion

At present, there are already adequate methods to monitor the water depth using satellite images. However, different monitoring methods are required for different water environments. In addition, most of the researches are focused on Case-I water where there are few human activities and water quality is excellent. Little research has been done for inland water areas. In response to these two points, this paper explores the feasibility of the bathymetry retrieval method, using the DII for substrate cluster in the Xia Shan Reservoir in China. According to the analysis of our experimental results, it is found that this bathymetry retrieval method can achieve a relatively high accuracy. This also demonstrates that retrieval methods generally used for the ocean can also apply to inland water. The application of this method will play a vital role in monitoring bathymetry and the environment of the Reservoir.

Nowadays, several researchers have conducted bathymetry retrieval without in-situ water depth data. For example, Yan Xu et al (Xu et al., 2023) conducted a study on bathymetric inversion without measured data for the South China Sea. Similarly, Liu et al (Liu et al., 2021) used high spatial resolution satellites to obtain bathymetric information in the absence of measured data, which provided great support for the study of optically shallow water areas of islands and reefs in the South China Sea. In this study, bathymetry retrieval is carried out using in-situ water depth data. It is hoped that bathymetry inversion without in-situ data can also be carried out in this area. This will greatly reduce the cost of environmental monitoring.

## 6. Conclusion

In this paper, the bathymetry of Xia Shan Reservoir is retrieved using GF-2 and Sentinel-2 images. DIIs are firstly applied to cluster the substrates into two or three clusters. Then, the Stumpf linear log-ratio model and the non-linear Legleiter model are used for bathymetry retrieval. GA algorithm is used to obtain the model parameters.

Experiments are as follows. First, the substrates are clustered into two or three clusters. According to the true color images, samples are selected from bright and dark pixels by visual interpretation. These samples are used to calculate  $k_i/k_j$  and DIIs, then a K-MEANS clustering algorithm is applied to cluster the substrate. After clustering, some in-situ samples are selected in GF-2 and Sentinel-2 images. Then, for bathymetry retrieval modeling, the GA optimization algorithm is applied to solve model parameters. At last, bathymetry results with two clusters, three clusters, and without substrates clusters are evaluated separately and compared to each other.

Based on the above experiments, it was found that, first of all, when there are various substrate types in the study area, the substrate cluster

before bathymetry retrieval is very necessary, it can improve the bathymetry retrieval accuracy significantly. For example, without cluster, the  $R^2$  values are all around 0.53 in the Sentienl-2 image, and the maximum RMSE and RRMSE values are 1.25 m and 26.21 %. While for the two clusters case using the Legleiter model, the  $R^2$  is improved to a maximum of 0.9 and RRMSE is reduced to a minimum of 11.76 %, the improvement is very obvious. For the three clusters case using the Legleiter model, the  $R^2$  increased to about 0.8, and RMSE reduced from 1.25 m to around 0.97 m, this also means better improvements. So, substrate clusters are very effective for improving bathymetry retrieval accuracy. Secondly, clustering substrates into more clusters may not necessarily improve retrieval accuracy, and how many substrate clusters need to be determined according to the actual situation. For example, in the two clusters case, using the Legleiter model in the GF-2 image, has the highest retrieval accuracy, where the RMSE is 0.76 m and the  $R^2$  is 0.9. However, when the bottom is divided into three clusters, using the same model, the  $R^2$  is reduced to 0.83 and the RMSE is increased to 0.99 m. This proves that the accuracy decreases with more substrate clusters. For our research area, it is obvious that there are bright and dark which can be determined from the true-color image. So, two clusters are suitable for our case, there is no necessity to divide the substrate into more clusters. This is also demonstrated by our experiment. In addition, the experiment also shows that the Legleiter model is more suitable for our research area. For example, for the two-cluster case, results using the Legleiter model are better than those of the Stumpf model. Using the Legleiter model, the  $R^2$  values are 0.9 and 0.78 respectively. When using the Stumpf model, the  $R^2$  values are 0.78 and 0.64 respectively.

In conclusion, when there are various bottom types exist in the study area, it is suggested to cluster the bottom before bathymetry retrieval. The number of bottom types should depend on the actual situation. Our research shows that substrate cluster using the DIIs and retrieving the bathymetry further using the non-linear Legleiter model is very effective and feasible in the Xia Shan Reservoir.

## CRediT authorship contribution statement

**Jinshan Zhu:** Supervision, Methodology. **Bopeng Liu:** Writing – original draft. **Yina Han:** Data curation. **Zhen Chen:** Funding acquisition. **Jianzhong Chen:** Data curation, Project administration. **Shijun Ding:** Data curation, Funding acquisition, Project administration. **Tao Li:** Data curation, Funding acquisition, Project administration.

## Declaration of competing interest

The authors declare that they have no known competing financial interests or personal relationships that could have appeared to influence the work reported in this paper.

## Acknowledgments

The authors would like to express their sincere gratitude to the Geological Exploration and Surveying Team of Shandong Bureau of Coal Geology for funding the project through Shandong Bureau of Coal Geology Special Funding for Scientific Research (No.45, 2022) and the Department of Science and Technology of Shandong Province for funding the project through Grant ZR2023MD082.

## References

- Ashphaq, M., Srivastava, P.K., Mitra, D., 2021. Review of near-shore satellite-derived bathymetric: Cluster and account of five decades of coastal bathymetric research. *J. Ocean. Eng. Sci.* 6 (4), 340–359. <https://doi.org/10.1016/j.joes.2021.02.006>.
- Bo, Y., Zhou, F., Zhao, J.S., et al., 2021. Additional surface-water deficit to meet global universal water accessibility by 2030. *J. Clean. Prod.* 320 <https://doi.org/10.1016/j.jclepro.2021.128829>.
- Cahalane, C., Magee, A., Monteys, X., 2019. A comparison of Landsat 8, RapidEye and Pleiades products for improving empirical predictions of satellite-derived

- bathymetry. *Remote Sens. Environ.* 233, 111414 <https://doi.org/10.1016/j.rse.2019.111414>.
- Chen, B.Q., Yang, Y.M., Xu, D.W., et al., 2019. A dual-band algorithm for shallow water depth retrieval from high spatial resolution imagery with no ground truth. *Isprs. J. Photogram.* 151, 1–13. <https://doi.org/10.1016/j.isprsjprs.2019.02.012>.
- Cheng, J., Ma, Y., Zhang, J.Y., 2021. Water-depth-zoning-inversion based on the relationship between two-band radiance data and the depth-invariant index. *Reg. Stud. Mar. Sci.* 44, May. <https://doi.org/10.1016/j.rsma.2021.101790>.
- Di, K.C., Ding, Q., Chen, W., Cao, W.Y., 1999. Shallow water depth extraction and chart production from tm images in nansha islands and nearby sea area. *Remote. Sens. Nat. Resour.* 11 (3), 59–64. <https://doi.org/10.3969/j.issn.1001-070X.1999.03.012>.
- Dimitris, P., Dimosthenis, T., Peter, R., et al., 2019. On the use of Sentinel-2 for coastal habitat mapping and satellite-derived bathymetry estimation using downsampled coastal aerosol band. *Int. J. Appl. Earth. Obs. Geoinf.* 80, 58–70. <https://doi.org/10.1016/j.jag.2019.03.012>.
- Goldberg, D.E., Holland, J.H., 1988. Genetic algorithms and machine learning. *Mach. Learn.* 3, 95–99. <https://doi.org/10.1023/A:1022602019183>.
- Guo, Z.F., Boeing, W., Borgomeo, E., et al., 2021. Linking reservoir ecosystems research to the sustainable development goals. *Sci. Total Environ.* 781, 4. <https://doi.org/10.1016/j.scitotenv.2021.146769>.
- Legleiter, C.J., 2021. The optical river bathymetry toolkit. *River Res. Appl.* 37 (4), 555–568. <https://doi.org/10.1002/rra.3773>.
- Liu, M.Y., Zhao, J., Deng, R.R., et al., 2021. A downsampled bathymetric mapping approach combining multitemporal Landsat-8 and high spatial resolution imagery: Demonstrations from clear to turbid waters. *Isprs. J. Photogramm.* 180, 65–81. <https://doi.org/10.1016/j.isprsjprs.2021.07.015>.
- Lyzenga, D., 1978. Passive remote-sensing techniques for mapping water depth and bottom features. *Appl. Opt.* 17 (3), 379–383. <https://doi.org/10.1364/AO.17.000379>.
- Ma, Y., Zhang, J., Zhang, J.Y., et al., 2018. Progress in optical remote sensing of shallow bathymetric. *Adv. Mar. Sci.* 36 (4), 331–351. <https://doi.org/10.3969/j.issn.1671-6647.2018.03.001>.
- Manseea, M.D.M., Haidar, M., Budhiman, S., et al., 2016. Evaluating the performance of Lyzenga's water column correction in case-1 coral reef water using a simulated Wolrdview-2 imagery. *IOP Conf. Ser.: Earth Environ. Sci.* 47 (1), 012018. <https://doi.org/10.1088/1755-1315/47/1/012018>.
- Manuputty, A., et al., 2017. The utilization of Depth Invariant Index and Principle Component Analysis for mapping seagrass ecosystem of Kotok Island and Karang Bongkok, Indonesia. *IOP Conf. Ser.: Earth Environ. Sci.* 54 <https://doi.org/10.1088/1755-1315/54/1/012083>, 012083.
- F. C. Polcyn, I. J. Sattinger, "Water Depth Determinations Using Remote Sensing Techniques," 1969.
- Polcyn, F.C., Lyzenga, D.R., 2013. Calculations of water depth from ERTS-MSS data. NASA. Goddard Space Flight Center Symp. on Significant Results obtained from the ERTS-1, vol. 1, Sect. A and B.**
- Reshitnyk, L., Costa, M., Robinson, C., Dearden, P., 2014. Evaluation of WorldView-2 and acoustic remote sensing for mapping benthic habitats in temperate coastal Pacific waters. *Remote. Sens. Environ.* 153, 7–23. <https://doi.org/10.1016/j.rse.2014.07.016>.
- Shang, Z.J., Jin, W.J., Xu, Z.F., et al., 2021. Research on 6S Mode of Atmospheric Correction for GF-1 Multispectral Image. *Radio Eng.* 51 (8), 705–710. <https://doi.org/10.3969/j.issn.1003-3106.2021.08.005>.
- Stumpf, R.P., Holderied, K., Sinclair, M., 2003. Determination of water depth with high-resolution satellite imagery over variable bottom types. *Limnol. Oceanogr.* 48 (1), 547–606. [https://doi.org/10.4319/lo.2003.48.1.part\\_2.0547](https://doi.org/10.4319/lo.2003.48.1.part_2.0547).
- Suo, L.L., Cai, L.Y., Sun, X., et al., 2019. Mapping coral reefs at Xisha Islands using Landsat8. *China Sciencetech Pap.* 14 (3), 347–352. <https://doi.org/10.3969/j.issn.2095-2783.2019.03.019>.
- WCD (World Commission on Dams), 2000. Dams and development: a framework for decision making. Earthscan, London, UK.**
- Xu, Y., Cao, B., Deng, R.R., et al., 2023. Bathymetric over broad geographic areas using optical high-spatial-resolution satellite remote sensing without in-situ data. *Int. J. Appl. Earth. Obs. Geoinf.* 119 <https://doi.org/10.1016/j.jag.2023.103308>.
- Zhao, W.J., Tamura, M., Takahashi, H., 2021. Atmospheric and spectral corrections for estimating surface albedo from satellite data using 6S code. *Remote Sens. Environ.* 76, 202–212. [https://doi.org/10.1016/S0034-4257\(00\)00204-2](https://doi.org/10.1016/S0034-4257(00)00204-2).
- Zhu, J.S., Yin, F., et al., 2022. Shallow water bathymetry retrieval by optical remote sensing based on depth-invariant index and location features. *Can. J. Remote Sens.* 48 (4), 534–550. <https://doi.org/10.1080/07038992.2022.2104235>.